Copyright © 2020 by American Scientific Publishers
All rights reserved.
Printed in the United States of America

AMERICAN SCIENTIFIC PUBLISHERS

Science of Advanced Materials
Vol. 12, pp. 1–10, 2020
www.aspbs.com/sam

ARTICLE

Influence of Sb_2O_3 Nanoparticles Addition on the Thermal, Microstructural and Creep Properties of Hypoeutectic Sn–Bi Solder Alloy

Alaa F. Abd El-Rehim[1,2,*], Ashraf S. Mahmoud[2], and Shereen M. Abdelaziz[2,3]

[1]*Physics Department, Faculty of Science, King Khalid University, Abha 61413, Saudi Arabia*
[2]*Physics Department, Faculty of Education, Ain Shams University, Heliopolis 11771, Roxy, Cairo, Egypt*
[3]*Physics Department, Faculty of Science, Qassim University, Buraydah 51452, Saudi Arabia*

ABSTRACT

Here we investigate the effects (thermal, microstructural, and creep properties) of adding Sb_2O_3 nanoparticles to a hypoeutectic Sn-5 wt% Bi solder alloy. The Sb_2O_3-containing solder alloy was prepared by mechanically incorporating 0.5 wt% Sb_2O_3 nanoparticles into the Sn-5 wt% Bi solder alloy. The addition of nano-sized Sb_2O_3 particles to the Sn–Bi solder alloy increases the melting temperature, but only slightly. The main phases of the investigated solder alloys include the β-Sn and Bi-rich phases in addition to the crystalline phase of Sb_2O_3 nanoparticles. No other intermetallic compounds were observed in the β-Sn matrix. The tensile creep experiments have been carried out in the 303–363 K temperature interval under constant stresses ranging from 5.1 to 7.64 MPa. The creep parameters of both solders increased gradually with increasing creep temperature up to 333 K, after which they increased rapidly with relatively higher values. The creep parameters of the Sb_2O_3-containing solder alloys are smaller than that of Sb_2O_3-free solder alloys. The present solder alloys exhibit class-M creep behavior. The calculated stress exponent values and activation energy data for both solders could be related to dislocation climb through core diffusion as the dominant operating mechanism.

KEYWORDS: Pb-Free Solder, Nanoparticle, Microstructure, Creep Properties.

1. INTRODUCTION

Recently, health and environmental issues about Pb toxicity have led to ban the use of Sn–Pb solder alloy in the electronics industry.[1,2] Among the many available Pb-free solders, Sn–Bi solder is a promising candidate because of its good mechanical properties, low melting temperature (that enables lower soldering temperature), and low thermal expansion coefficient.[3,4]

Several reports have documented the properties of Sn–Bi solder alloys under various test conditions. Mahmudi et al.[5] studied the creep characteristics of Sn–Bi solders using various Bi concentrations (1–5 wt%) using the long time Vickers indentation technique. These authors concluded that the creep strength improved with an increasing Bi ratio due to the solid solution hardening effects of the Bi-rich phase in the β-Sn matrix. Ye et al.[6] investigated the hardness and bending property of Sn–xBi solders ($x = 3.6$, 7.25, 14.5, 29, and 58 wt%). The changes in hardness and bending property were explained considering the variations in the volume fraction and morphology of the Bi-rich phase within the β-Sn matrix. The creep properties of Sn–xBi solders ($x = 1$, 2, and 5 wt%) have been studied using the conventional tensile creep tests, and the creep strength was enhanced with the increase in the Bi concentration.[7]

There are some drawbacks of Sn–Bi solders, such as coarsening microstructure during thermal aging, which would degrade the joining property of the Sn–Bi solders.[8,9] Consequently, it is essential to discover how to improve their brittleness and refine their microstructures. It is well accepted[10–12] that the addition of second reinforcing nano-sized particles is a powerful method to promote the creep resistance and mechanical features of solders due to the microstructure modifications. The mechanical characteristics and microstructure evolutions of eutectic Sn-58 wt% Bi solder reinforced with nano-sized SiC particles have been investigated.[13] The addition of SiC refined the microstructure of β-Sn matrix and promoted the shear strength of the binary eutectic solder. Yang et al.[14] inspected the microstructural development and mechanical

*Author to whom correspondence should be addressed.
Email: alaa.abdelrehim@kku.edu.sa
Received: 19 October 2019
Revised/Accepted: 29 March 2020

ARTICLE

properties of Sn–58Bi solder reinforced with different contents of $BaTiO_3$ nanoparticles. These authors found that the microstructure is refined with increasing $BaTiO_3$ content that provides heterogeneous nucleation sites in the matrix. The best mechanical properties have been achieved at a $BaTiO_3$ concentration of 1 wt%. Lü et al.[15] concluded that the addition of Ag nanopowders to Sn–58Bi solder significantly improved the mechanical properties of the solder. This behavior was ascribed to the effective refinement of the microstructure of the β-Sn matrix and formation of Ag_3Sn intermetallic compound (IMC). Liu et al.[16] examined the melting temperature of the Sn-58Bi solder reinforced with various concentrations of Y_2O_3 nanoparticles. These authors also indicated that the melting temperatures slightly increased with an increase in the ratio of Y_2O_3 nanoparticles. Ma et al.[17] reported that the addition of graphene nanosheets into the Sn–58Bi solder enhanced the tensile properties, hardness, and creep characteristics.

Despite the above findings concerning the microstructure development and mechanical features of Sn–Bi solder alloys, the correlations between the microstructure development and mechanical properties of hypoeutectic Sn-5 wt% Bi solder reinforced with nano-sized Sb_2O_3 particles have not been addressed in the literature. Therefore, the present work is devoted to exploring the impact of adding Sb_2O_3 nanoparticles to hypoeutectic Sn-5 wt% Bi solder.

2. EXPERIMENTAL DETAILS

In this work, we used nominally spherical Sb_2O_3 nanoparticles (99.98% purity) with an average particle size that ranged from 20 to 100 nm. The spherical shape morphology of Sb_2O_3 nanoparticles was confirmed by SEM investigation (Fig. 1(a)). Analysis of X-ray diffraction (XRD) was carried out for phase identification of Sb_2O_3 nanoparticles (Fig. 1(b)). It is worth noting that the nano-sized Sb_2O_3 particles appeared in crystalline phases with sharp peaks in accordance with JCPDS card No. 72-1854.

Commercially available pure Sn and Bi were used to produce the Sn-5 wt% Bi solder (designated solder A). The Sn-5 wt% Bi-0.5 wt% Sb_2O_3 solder (designated solder B) was prepared by mechanically incorporating 0.5 wt% of Sb_2O_3 nanoparticles into the Sn-5 wt% Bi master solder. The solder B was remelted at 673 K for 30 min in an electric resistance furnace under a protective argon atmosphere, and then the melt was poured into a metal mold in the air at 298 K (room temperature). The chemical composition of the prepared solders was analyzed by inductively coupled plasma atomic emission spectroscopy (ICP-AES) (Table I). For tensile creep measurements, wires of 0.8 mm gauge diameter and 50 mm gauge length machined from the casting ingots were solution-heat-treated at 448 K for 2 h followed by water quenching into iced water at 273 K. The temperature measurements accuracy was $\pm$1 K.

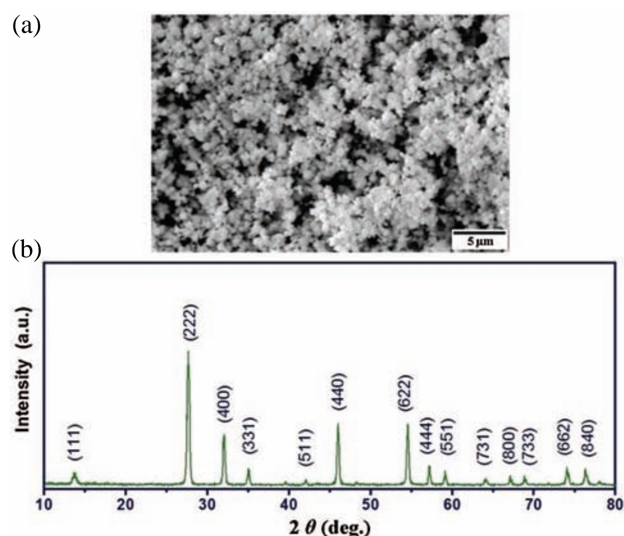

Fig. 1. (a) SEM micrograph of the nano-sized Sb_2O_3 particles, (b) X-ray diffraction spectra of the nano-sized Sb_2O_3 particles.

The tensile creep tests were done using an Instron 3360 Universal Testing Machine in the 303 to 363 K temperature interval under constant stresses (from 5.1 to 7.64 MPa). The details of the tensile testing machine are described elsewhere.[18] The tensile creep measurements were performed in the temperature region where there is a single phase (solid solution of Bi in β-Sn matrix).

To examine the microstructure of samples, they were ground and polished following the typical steps carried out for solder alloys. To reveal the grain boundaries, a solution comprising of 4 ml HNO_3 and 96 ml C_2H_5OH was used to etch the samples for about 60 s. The as-cast microstructure of these solders was studied by means of scanning electron microscope (SEM, JSM-6360LV) equipped with an energy dispersive spectroscope (EDS) operating at 20 kV. Phase constitutions of the investigated soldiers were analyzed by means of X-ray diffraction (XRD, Shimadzu D6000 with Ni-filtered CuKα radiation ($\lambda = 1.5406$ Å)).

To assess the melting characteristics of both solders, differential scanning calorimetry (DSC) experiments have been carried out using a TA Instruments-Q10 DSC apparatus. Each sample of 10 mg was placed into an Al pan and heated at a rate of 10 °C/min under the flow of N_2 gas.

Table I. Chemical composition of the experimental solder alloys analyzed by an inductively coupled plasma atomic emission spectroscopy (ICP-AES), wt.%.

	Element content		
Solder	Bi	Sb_2O_3	Sn
Sn–5Bi (solder A)	4.92	0	Bal.
Sn–5Bi–0.5Sb_2O_3 (solder B)	4.86	0.47	Bal.

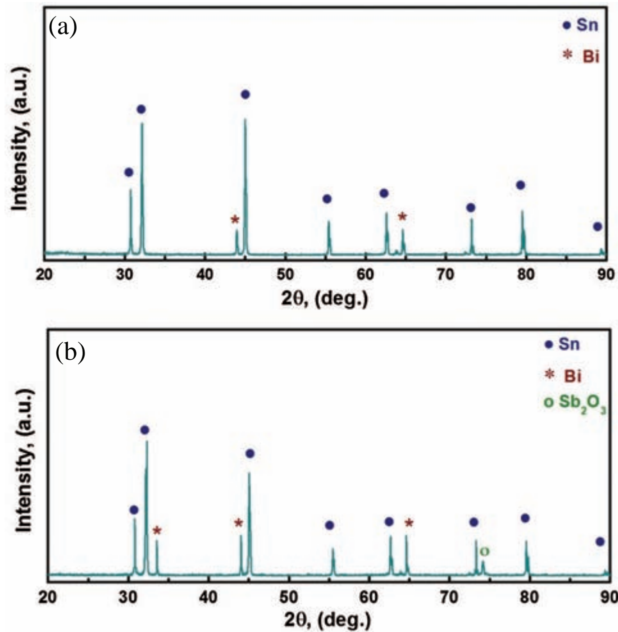

Fig. 2. XRD patterns of the as-cast (a) solder A and (b) solder B.

3. RESULTS AND DISCUSSION

3.1. Microstructure Observations

To identify the initial phases, the as-cast microstructure of solders A and B was investigated by XRD at room temperature (Fig. 2). It is worth noting that the microstructure of solder A consists primarily of Bi-rich and Sn-rich phases that are identified by comparison with JCDPS cards No. 85-1331 and No. 4-0673, respectively (Fig. 2(a)). Meanwhile, the solder B exhibited an extra peak of Sb_2O_3 along with peaks of Bi-rich and Sn-rich phases (Fig. 2(b)). The crystalline phase of Sb_2O_3 was matched using JCPDS card No. 72-1854. This implies that the nano-sized Sb_2O_3 particles were actually in solder B.

Two SEM images showing the as-cast microstructure of solders A and B are presented in Figure 3. The main constitutions are the Bi-rich phase (white phase) and the β-Sn phase (dark gray phase). It is inferred that the precipitated Bi particles were accumulated within the β-Sn matrix. This microstructure is comparable to those reported previously in the literature.[5] The EDS data confirmed that the white phase is the Bi-rich phase, and the dark gray phase is the β-Sn phase. It can be concluded from the comparison of the micrographs in Figure 3 that the microstructure is identical, but the volume fraction of the Bi-rich phase is varied. The volume fraction of fine Bi particles in the solder B is denser than that of solder A. This might be ascribed to the presence of Sb_2O_3 nanoparticles that provides more nucleation sites for the Bi particles. This is in line with the previous work of Yang et al.,[19] who found that the addition of Al particles to Sn–Bi solder enhanced the precipitation of the Bi-rich phase. Mokhtari and Nishikawa[20] reported that the volume fraction of the Bi-rich phase increased with increasing Sb content in the Sn–Bi–Sb solders. Mahmudi et al.[21] studied the microstructural development of Sn–2Bi solder reinforced with Ce and La as rare earth elements (REs). These authors concluded that the volume fraction of the Bi-rich

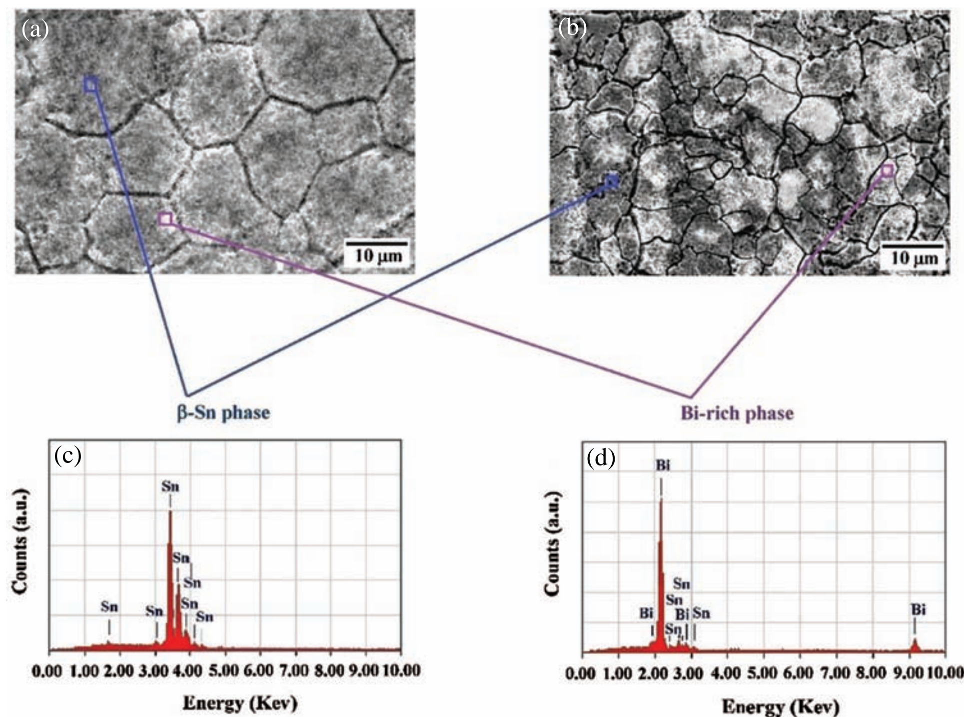

Fig. 3. Microstructure and corresponding EDS spectra of (a) solder A, (b) solder B, (c) β-Sn phase, and (d) Bi-rich phase.

ARTICLE

ARTICLE

phase in the Sn–Bi solders containing 0.1 REs is higher than that of the REs-free solders. A higher magnification SEM micrograph of solder B reinforced with Sb_2O_3 nanoparticles is presented in Figure 4. It is evident that the nano-sized Sb_2O_3 particles are homogenously distributed without aggregation within the β-Sn matrix.

3.2. Thermal Analysis

Figure 5 displays the DSC curves of both solders during heating at 10 °C/min. The melting characteristics were collected and summarized in Table II. From Figure 5, only one single sharp endothermic peak corresponding to the melting reaction was noticed for each solder. During the melting process of solders, no phase transition was observed. Table II illustrates that the melting temperature of solder A increases slightly from 230.4 °C to 230.6 °C with the addition of Sb_2O_3. This observation is consistent with other reports on Sn-based solders.[10,22,23] Gain et al.[24,25] reported that the addition of ZrO_2 nanoparticles to the Sn–Ag–Cu (SAC) solder shifted the melting temperature from 217 °C to 217.3 °C, while the melting temperature of SAC solder bearing TiO_2 nanoparticles ranged from 217 to 217.6 °C. Yakymovych et al.[26] reported that the melting peak of SAC solder reinforced with nano-sized Co changed slightly by about 0.5 °C for a Co addition of 0.6 wt%. El-Daly and Hammad[27] concluded that the addition of 1.5 wt% Ag to the Sn–9Zn solder has little impact on the melting point, which is less than 0.4 °C. This is possibly because the addition of Sb_2O_3 nanoparticles to the Sn–Bi solder modifies the physical characteristics of grain boundary/interfacial properties and alters the surface instability.[28] The pasty range of two solders varies from 8.9 to 9.2 °C, which is lower than 11 °C for the eutectic Sn–Pb solder. This small pasty range can reduce the possibility of functional solder towards hot tearing and porosity as a result of the influence of solder shrinkage.[29] For these reasons, the Sn–Bi solders reinforced with Sb_2O_3 nanoparticles have shown satisfactory reliability.

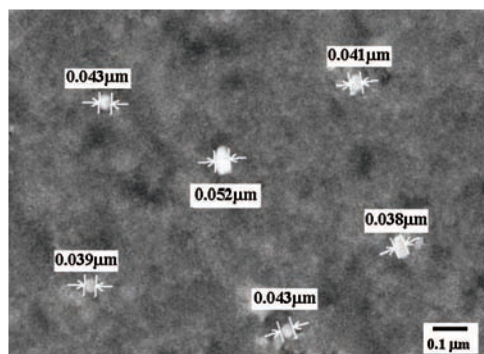

Fig. 4. Typical SEM micrograph showing the distribution of Sb_2O_3 nanoparticles within the solder B.

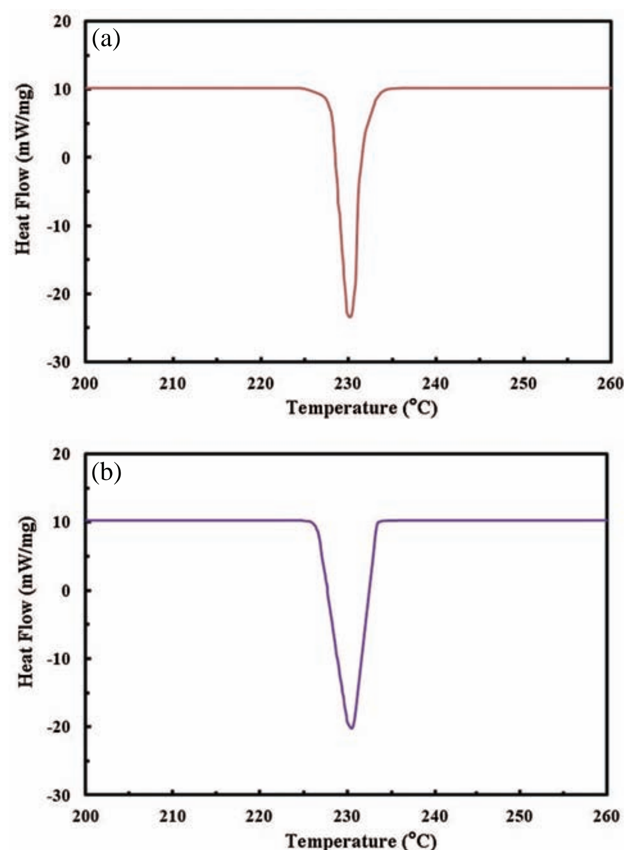

Fig. 5. DSC results of (a) solder A and (b) solder B.

3.3. Creep Properties

Figure 6 shows representative creep curves of both solders A and B crept in the temperature interval of 303–363 K under constant stresses ranging from 5.1 to 7.64 MPa. It is noteworthy that all creep curves show normal creep behavior with three different phases: (i) transient creep stage corresponds to a decay of the creep strain rate with time; (ii) steady-state creep stage describes a quasi-constant creep strain rate; and (iii) tertiary creep stage where the creep strain rate accelerates to fracture.[30] Inspection of these sets of curves shows that the creep rate values are shifted monotonically towards higher values with increasing creep temperature, T, and/or applied stress, σ. Moreover, the values of the creep strain rate of solder B are smaller than that of solder A.

Table II. Solidus temperature (T_S), liquidus temperature (T_L), melting temperature (T_m) and pasty range (ΔT) of both solders A and B.

Solder	T_m (°C)	T_L (°C)	T_s (°C)	ΔT (°C)
Solder A	230.4	233.7	224.8	8.9
Solder B	230.6	234.4	225.2	9.2

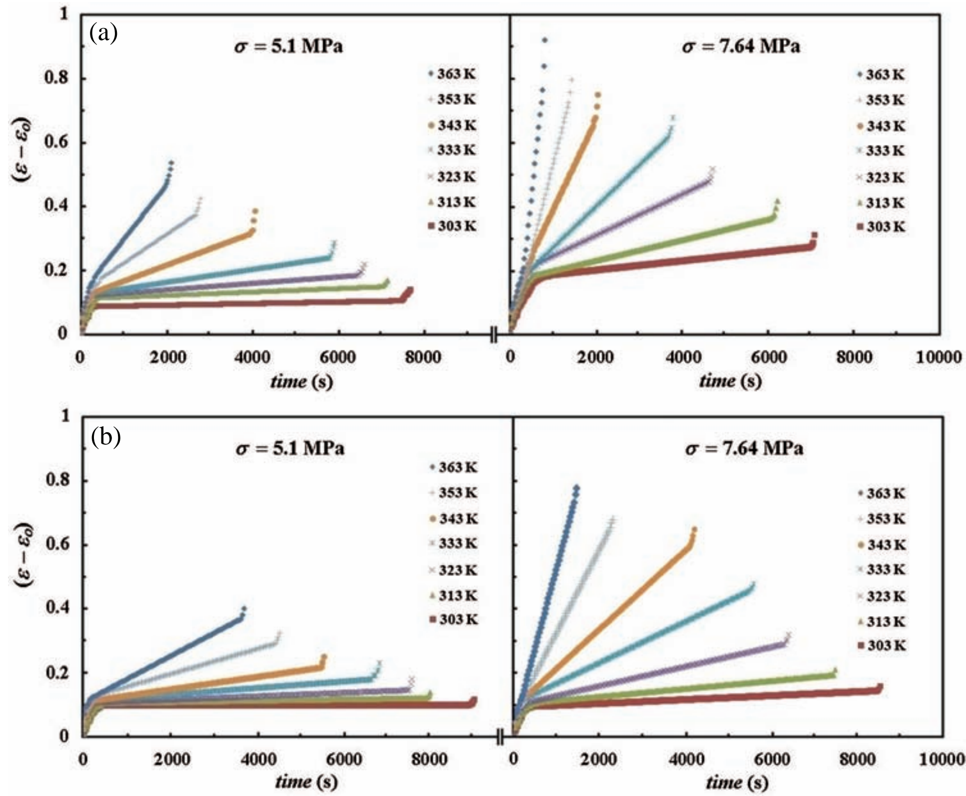

Fig. 6. Representative creep curves for (a) solder A and (b) solder B under constant applied stresses as indicated. ε_o is the instantaneous creep at time = 0.

The transient creep strain, ε_{tr}, can be described by the power-law relationship:[31,32]

$$\varepsilon_{tr} = \lambda(t_{tr})^{\alpha} \tag{1}$$

where λ and α are the transient creep parameters of the material that depend on stress and temperature. t_{tr} is the transient creep time in seconds. At each creep temperature, the gradient of $\ln \varepsilon_{tr}/\ln t_{tr}$ plots gives the value of the parameter α. The parameter λ was evaluated by substitution in the equation:

$$\lambda = \frac{\ln t_2 \ln \varepsilon_{tr1} - \ln t_1 \ln \varepsilon_{tr2}}{\ln t_2 - \ln t_2} \tag{2}$$

which is derived from Eq. (1). The creep temperature dependence of both α and λ parameters under various applied stresses for both solders is shown in Figures 7 and 8, respectively. The values of steady-state creep rate,

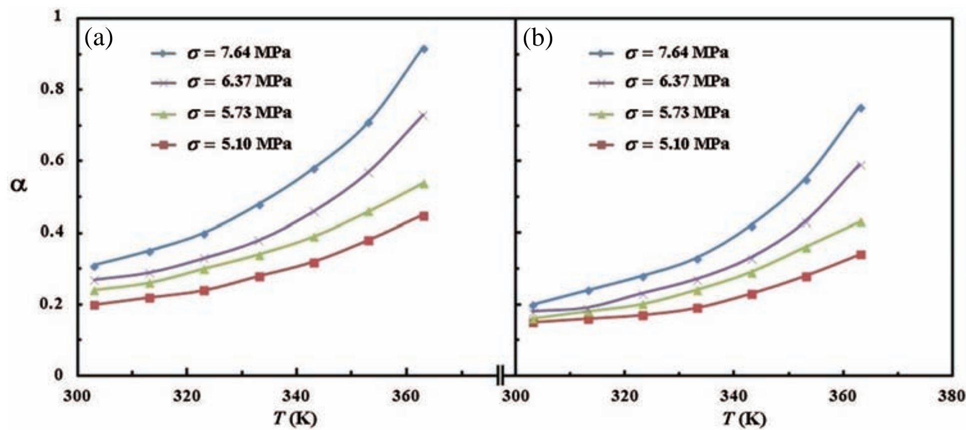

Fig. 7. Dependence of the transient creep parameter, α, on the creep temperature, T, for (a) solder A and (b) solder B under different applied stresses, σ.

ARTICLE

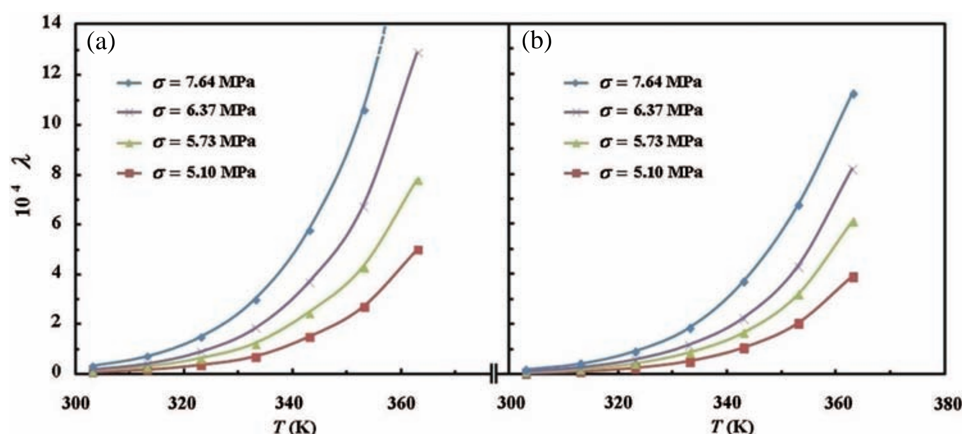

Fig. 8. Dependence of the transient creep parameter, λ, on the creep temperature, T, for (a) solder A and (b) solder B under different applied stresses, σ.

$\acute{\varepsilon}_{st}$, were estimated from the slopes of the linear parts of the obtained creep curves presented in Figure 6. Figure 9 depicts the dependence of the $\acute{\varepsilon}_{st}$ on the creep temperature under various applied stresses for both solders. From Figures 7–9, it is seen that the values of the creep parameters α, λ, and $\acute{\varepsilon}_{st}$ of both solders increased gradually with increasing creep temperature up to 333 K, after which they increased rapidly with relatively higher values.

The binary phase diagram of the Sn–Bi system shows two equilibrium phases at room temperature: Sn-rich phase (β-Sn) and Bi-rich phase (Fig. 10). The solid solubility of Bi in the β-Sn matrix peaks (21 wt%) at 139 °C (eutectic temperature). The dashed vertical line in Figure 10 represents the investigated composition of the solders studied in the current work. During the solidification process, the second phase (Bi solid solute atoms) will start to precipitate from the solid solution phase. The final microstructure is composed of finely dispersed Bi particles within the β-Sn matrix. The gradual increase of the creep parameters in the creep temperature interval of 303–333 K, under different applied stresses for both solders A and B, could be rendered as being due to the coarsening process of Bi atoms to form a Bi-rich phase. Subsequently, the interaction between the Bi solute atoms and the stress fields of moving dislocations will be reduced, resulting in higher creep parameters. Our experimental data agree with those reported by Al-Ganainy and co-workers,[33] who pointed out that the values of creep parameters are enhanced at creep temperatures ranging from 305 to 328 K. In the creep temperature interval (333–363 K), the creep parameters for both solders increased quickly with relatively higher values. This trend could be explained in view of the binary phase diagram of the Sn–Bi system (Fig. 10). The solid solubility of Bi in the β-Sn-phase is about 10 wt% at 373 K. The Bi atoms can, therefore, be completely dissolved at 333 K in the β-Sn-phase. As the temperature rises from 333 to 363 K, all Bi atoms are absorbed by the β-Sn-phase, which is converted into the β-Sn-rich phase. Consequently, there will be no Bi-rich phase, and thus, with increasing creep temperature, the creep parameters of both solders increase rapidly.

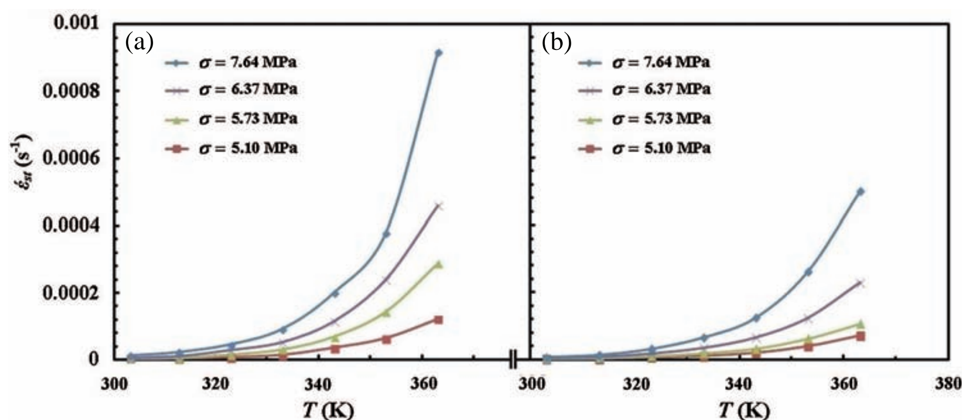

Fig. 9. Dependence of the steady state creep rate, $\acute{\varepsilon}_{st}$, on the creep temperature, T, for (a) solder A and (b) solder B under different applied stresses, σ.

ARTICLE

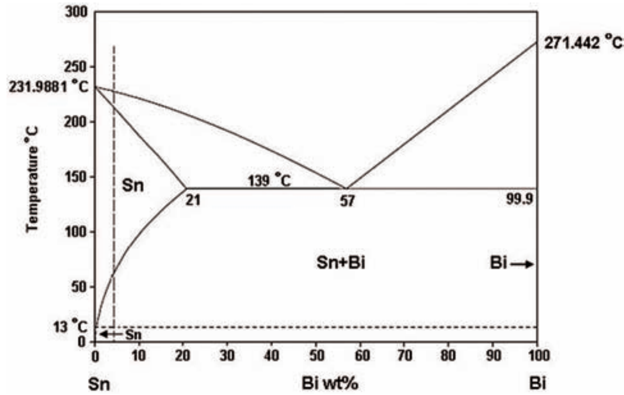

Fig. 10. The binary phase diagram of Sn–Bi system showing the concentration evaluated in this study.

The enhancement of the creep parameters of both solders with increasing applied stress at different creep temperatures may be elucidated in view of the consecutive mechanism. At the beginning of the creep test, the deformed samples contain a large number of dislocations that move across their glide planes. The movement of dislocation segments is resisted by internal stress arising from the Bi solute atoms. Thus, the segments will move only when the applied stress on it overcomes the internal stress. Increasing applied stress will provide the segments with the energy needed to climb and surpass these obstacles. Consequently, the creep parameters increase with increasing applied stress.

Comparing the creep parameters of both solders under the same test conditions, the creep parameters of solder B are smaller than those of solder A. Our experimental results agree with those reported by Yang et al.[34] who stated that the addition of nano-sized graphite reinforcement to the Sn–Bi solder drastically improved the creep resistance of the binary solder. During the solidification process of solder B, the β-Sn matrix cannot be wetted by nano-sized Sb_2O_3 particles because they are non-reactive and non-coarsening and do not form intermetallic compounds in the solder matrix. Therefore, the dispersed Sb_2O_3 nanoparticles within the Sn-matrix impedes grain boundary sliding and prevents the slipping of dislocations resulting in better creep resistance of the solder B, which agrees well with the dispersion strengthening theory.[35] Our observations are in line with those previously reported by other investigators on different solders.[10, 11, 36, 37]

Determining the activation energy magnitude of the creep process is a popular approach to determining the mechanisms controlling the deformation process. To estimate the transient activation energy, Q_{tr}, the parameter λ was presumed to satisfy the Arrhenius-type form:[32, 38]

$$\lambda = \text{constant } e^{-Q_{tr}/RT} \tag{3}$$

where R is the universal gas constant, and T is the creep temperature in Kelvin. The slopes of the isostress straight lines relating $\ln\lambda$ against $(1000/T)$ were computed, giving the Q_{tr} for both solders (Fig. 11). For both solders, the mean value of activation energy was found to be ~74.5 kJ/mol.

It is well accepted[39, 40] that the $\acute{\varepsilon}_{st}$ shows a strong dependence on the temperature of creep, T, and applied stress, σ. The $\acute{\varepsilon}_{st}$ is related to the σ by the simplified Dorn power-law relationship:[40]

$$\acute{\varepsilon}_{st} = B\sigma^n e^{-Q_{st}/RT} \tag{4}$$

where B is a constant, n is the stress exponent, and Q_{st} is energy activating the steady-state creep process. Presuming that only one mechanism governs the deformation behavior in the applied stress range, Eq. (4) yields:

$$\ln \acute{\varepsilon}_{st} = \ln B + n \ln \sigma - \frac{Q_{st}}{RT} \tag{5}$$

The n and Q_{st} are calculated by a linear best fit of Eq. (5) to the experimental creep data. Figure 12 depicts a linear relationship between the $\acute{\varepsilon}_{st}$ and the σ (both on logarithmic scales) for both solders at different creep

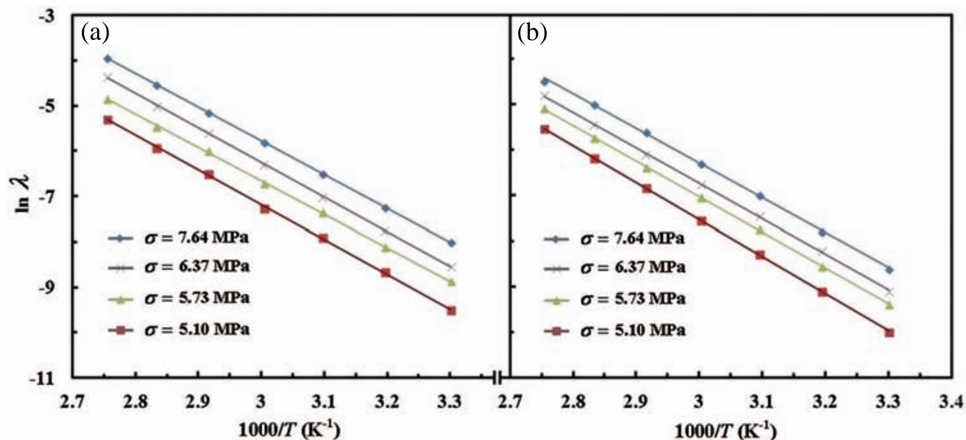

Fig. 11. A plot relating $\ln\lambda$ versus $1000/T$ for (a) solder A and (b) solder B under different applied stresses, σ.

ARTICLE

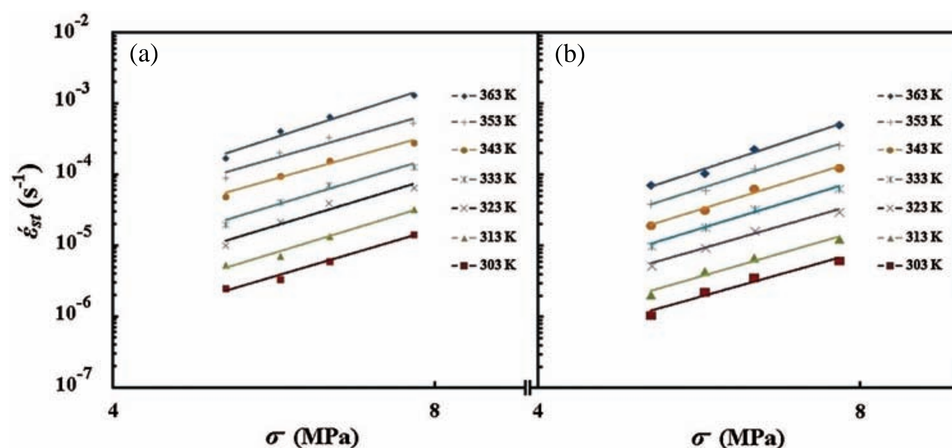

Fig. 12. Double-log plots of steady state creep rate, $\acute{\varepsilon}_{st}$, versus applied stress, σ, for (a) solder A and (b) solder B at different creep temperatures, T.

temperatures. The slopes of the straight lines fitted to the data give the n. The average value of n for both solders was 5.1. This value of stress exponent is in excellent agreement with the published creep results for Sn-based solders earlier disclosed.[2,7,40] The values of Q_{st} for both solders could be estimated from the plot of $\ln \acute{\varepsilon}_{st}$ against $1000/T$ (Fig. 13). For both solders A and B, the present results gave mean values of 73.6 and 78.2 kJ mol^{-1}, respectively. A review of studies on the available creep data of Sn-based solders in the solid solution range demonstrates a broad range in published activation energies and stress exponents.[4,41–43]

It has been reported[44] that the creep behavior of solid solution materials can be categorized into two classes: class I (also known as class A alloys type) and class II (also known as class M metals type). Most solid solution alloys show class M behavior. Class A alloys have a stress exponent of 3, which is found when solute atmospheres from around dislocations, with solute/dislocation interaction favored by large size differences between the solute and solvent atoms. The creep rate is then controlled by the rate at which the dislocations can move, dragging their solute atmospheres (i.e., the creep rate depends on the density of moving dislocations and their average velocity). Class A alloys do not display notable primary creep. The rate-control mechanism is assumed to be the dislocation climb when the stress exponent varies from 5 to 7 (class M metals). Since the creep properties of pure metals are essentially unaffected by the solute addition, no change in creep mechanism is involved, although solute atoms are present in the parent lattice. Class M metals typically display significant transient creep. Based on the creep characteristics of Sn–Bi solders, Mitlin et al.[7] classified the rate-controlling creep mechanisms into low temperature creep behavior (T < 120 °C) and high temperature creep behavior (T M 150 °C) with a transition region in between. The climb of dislocations—controlled by lattice diffusion with activation energy equal to the self-diffusion activation energy of bulk Sn (105–109 kJ/mol)—is the rate-controlling mechanism at high temperature creep behavior.[45] The climb of dislocations is dominated by the core diffusion process when the activation energy falls within the range of 30–70% of the self-diffusion energy. Sn is the predominant creep mechanism at a

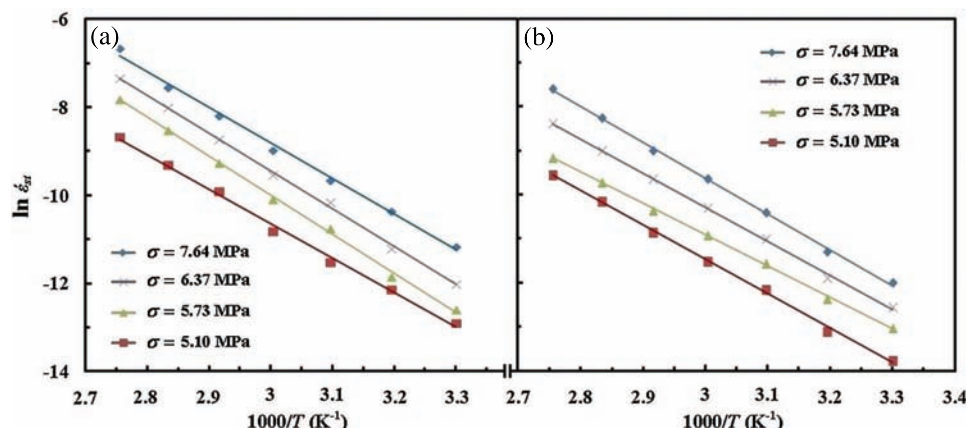

Fig. 13. A plot relating $\ln \acute{\varepsilon}_{st}$ versus $1000/T$ for (a) solder A and (b) solder B under different applied stresses, σ.

ARTICLE

low-temperature creep. In the present work, the activation energies of both transient and steady-state creep for both solders are around 0.68-times the activation energy of the self-diffusion energy of pure Sn. Together with the n of 5.1, it is assumed that the dominant creep deformation mechanism of both solders is dislocation climb through core diffusion at low temperature creep.

4. CONCLUSIONS

1. The addition of Sb_2O_3 nanoparticles increases the melting point of solder A, but only slightly.
2. The microstructure of solder A is refined with the addition of nano-sized Sb_2O_3 particles. This could be attributed to the presence of Sb_2O_3 nanoparticles, which provides heterogeneous nucleation sites in the β-Sn matrix.
3. The values of creep parameters of both solders increased slowly with creep temperature up to 333 K, after which they increased quickly with relatively higher values.
4. Solder B has a better creep resistance than solder A.
5. The calculated values of stress exponent and activation energy of both solders could be related to dislocation climb through core diffusion as the dominant operating mechanism.

Acknowledgments: The authors extend their appreciation to the Deanship of Scientific Research at King Khalid University for funding this work through research groups program under grant number R.G.P. 1/60/39.

References and Notes

1. L. M. Satizabal, D. Costa, P. B. Moraes, A. D. Bortolozo, and W. R. Osório, Microstructural array and solute content affecting electrochemical behavior of SnAg and SnBi alloys compared with a traditional SnPb alloy. *Mater. Chem. Phys.* 223, 410 (**2019**).
2. A. F. Abd El-Rehim, H. Y. Zahran, and S. AlFaify, The mechanical and microstructural changes of Sn–Ag–Bi solders with cooling rate and Bi content variations. *J. Mater. Eng. Perform.* 27, 344 (**2018**).
3. Y. Ma, X. Li, L. Yang, W. Zhou, M. Wang, W. Zhu, and P. Wu, Effects of graphene nanosheets addition on microstructure and mechanical properties of SnBi solder alloys during solid-state aging. *Mater. Sci. Eng., A* 696, 437 (**2017**).
4. L. Shen, P. Septiwerdani, and Z. Chen, Elastic modulus, hardness and creep performance of SnBi alloys using nanoindentation. *Mater. Sci. Eng., A* 558, 253 (**2012**).
5. R. Mahmudi, A. R. Geranmayeh, S. R. Mahmoodi, and A. Khalatbari, Room-temperature indentation creep of lead-free Sn–Bi solder alloys. *Journal of Materials Science: Materials in Electronics* 18, 1071 (**2007**).
6. D. Ye, C. Du, M. Wu, and Z. Lai, Microstructure and mechanical properties of Sn–*x*Bi solder alloy. *Journal of Materials Science: Materials in Electronics* 26, 3629 (**2015**).
7. D. Mitlin, C. H. Raeder, and R. W. Messler, Solid solution creep behavior of Sn–*x*Bi alloys. *Metallurgical and Materials Transactions: A* 30, 115 (**1999**).
8. X. Chen, F. Xue, J. Zhou, and Y. Yao, Effect of In on microstructure, thermodynamic characteristic and mechanical properties of Sn–Bi based lead-free solder. *J. Alloys Compd.* 633, 377 (**2015**).
9. W. Dong, Y. Shi, Z. Xia, Y. Lei, and F. Guo, Effects of trace amounts of rare earth additions on microstructure and properties of Sn–Bi-based solder alloy. *J. Electron. Mater.* 37, 982 (**2008**).
10. A. F. Abd El-Rehim, H. Y. Zahran, and A. M. Yassin, Microstructure evolution and tensile creep behavior of Sn–0.7Cu lead-free solder reinforced with ZnO nanoparticles. *Journal of Materials Science: Materials in Electronics* 30, 2213 (**2019**).
11. E. A. Eid, A. B. El-Basaty, A. M. Deghady, S. Kaytbay, and A. Nassar, Influence of nano-metric Al_2O_3 particles addition on thermal behavior, microstructural and tensile characteristics of hypoeutectic Sn–5.0Zn–0.3Cu Pb-free solder alloy. *Journal of Materials Science: Materials in Electronics* 30, 4326 (**2019**).
12. L. Zhang and K. N. Tu, Structure and properties of lead-free solders bearing micro and nano particles. *Materials Science and Engineering R* 82, 1 (**2014**).
13. C. W. Lee, Y. S. Shin, and S. H. Yoo, Effect of SiC nanoparticles dispersion on the microstructure and mechanical properties of electroplated Sn–Bi solder alloy. *Journal of Nano Research* 11, 113 (**2010**).
14. L. Yang, J. Dai, Y. Zhang, Y. Jing, J. Ge, and H. Liu, Influence of $BaTiO_3$ nanoparticle addition on microstructure and mechanical properties of Sn–58Bi solder. *J. Electron. Mater.* 44, 2473 (**2015**).
15. X. C. Lü, P. He, F. Pan, B. Du, F. J. Lu, and Y. Y. Qian, Effect of Ag nanopowders on microstructure, hardness and elastic modulus of Sn–Bi solders. *Engineering Review* 34, 63 (**2014**).
16. X. Liu, M. Huang, C. M. L. Wu, and L. Wang, Effect of Y_2O_3 particles on microstructure formation and shear properties of Sn–58Bi solder. *Journal of Materials Science: Materials in Electronics* 21, 1046 (**2010**).
17. Y. Ma, X. Li, W. Zhou, L. Z. Yang, and P. Wu, Reinforcement of graphene nanosheets on the microstructure and properties of Sn58Bi lead-free solder. *Mater. Des.* 113, 264 (**2017**).
18. A. M. Yassin, H. Y. Zahran, and A. F. Abd El-Rehim, Effect of TiO_2 nanoparticles addition on the thermal, microstructural and room-temperature creep behavior of Sn-Zn based solder. *J. Electron. Mater.* 47, 6984 (**2018**).
19. W. Yang, J. Li, J. Feng, J. Wu, X. Zhou, A. Yu, J. Wang, S. Liang, M. Wei, and Y. Zhan, Effect of aluminum addition on the microstructure and properties of non-eutectic Sn–20Bi solder alloys. *Materials* 12, 1194 (**2019**).
20. O. Mokhtari and H. Nishikawa, Correlation between microstructure and mechanical properties of Sn–Bi–*X* solders. *Mater. Sci. Eng., A* 651, 831 (**2016**).
21. R. Mahmudi, A. R. Geranmayeh, M. Salehi, and H. Pirayesh, Impression creep of the rare-earth doped Sn–2%Bi lead-free solder alloy. *Journal of Materials Science: Materials in Electronics* 21, 262 (**2010**).
22. S. Y. Chang, C. C. Jain, T. H. Chuang, L. Feng, and L. C. Tsao, Effect of addition of TiO_2 nanoparticles on the microstructure, microhardness and interfacial reactions of Sn3.5Ag*X*Cu solder. *Mater. Des.* 32, 4720 (**2011**).
23. M. Ahmed, T. Fouzder, A. Sharif, A. K. Gain, and Y. C. Chan, Influence of Ag micro-particle additions on the microstructure, hardness and tensile properties of Sn–9Zn binary eutectic solder alloy. *Microelectronics Reliability* 50, 1134 (**2010**).
24. A. K. Gain, T. Fouzder, Y. C. Chan, and W. K. C. Yung, Microstructure, kinetic analysis and hardness of Sn–Ag–Cu-1 wt% nano-ZrO_2 composite solder on OSP-Cu pads. *J. Alloys Compd.* 509, 3319 (**2011**).
25. A. K. Gain, Y. C. Chan, and W. K. C. Yung, Microstructure, thermal analysis and hardness of a Sn–Ag–Cu-1 wt% nanoTiO_2 composite solder on flexible ball grid array substrates. *Microelectronics Reliability* 51, 975 (**2011**).
26. A. Yakymovych, S. Mudry, I. Shtablavyi, and H. Ipser, Effect of nano Co reinforcements on the structure of the Sn–3.0Ag–0.5Cu solder in liquid and after reflow solid states. *Mater. Chem. Phys.* 181, 470 (**2016**).
27. A. A. El-Daly and A. E. Hammad, Elastic properties and thermal behavior of Sn–Zn based lead-free solder alloys. *J. Alloys Compd.* 505, 793 (**2010**).

ARTICLE

28. M. I. I. Ramli, N. Saud, M. A. A. Mohd Salleh, M. N. Derman, and R. Mohd Said, Effect of TiO_2 additions on Sn–0.7Cu–0.05Ni lead-free composite solder. *Microelectronics Reliability* 65, 255 (**2016**).

29. A. A. El-Daly, A. E. Hammad, G. A. Al-Ganainy, and A. A. Ibrahiem, Enhancing mechanical response of hypoeutectic Sn–6.5Zn solder alloy using Ni and Sb additions. *Mater. Des.* 52, 966 (**2013**).

30. A. F. Abd El-Rehim, Effect of grain size on the primary and secondary creep behavior of Sn-3 wt.% Bi alloy. *Journal of Materials Science* 43, 1444 (**2008**).

31. M. A. Mahmoud, A. F. Abd El-Rehim, A. M. Abd El-Khalek, A. H. Ashry, and G. Graiss, Study of precipitates formation in Al-4.5 wt% Cu and Al-4.5 wt% Cu-0.1 wt% in alloys using creep measurements and positron annihilation technique. *Cryst. Res. Technol.* 40, 665 (**2005**).

32. A. F. Abd El-Rehim, M. M. El-Sayed, M. R. Nagy, and M. Abd El-Hafez, Influence of quenching conditions on the mechanical and structural properties of Al-30 wt% Zn alloy. *Mater. Sci. Eng., A* 602, 105 (**2014**).

33. G. S. Al-Ganainy, B. A. Khalifa, R. Afify, and M. R. Nagy, Effect of phase transformation on creep characteristics of Sn-5 wt% Bi alloy. *Physica Status Solidi (a)* 158, 463 (**1996**).

34. L. Yang, C. Du, J. Dai, N. Zhang, and Y. Jing, Effect of nanosized graphite on properties of Sn–Bi solder. *Journal of Materials Science: Materials in Electronics* 24, 4180 (**2013**).

35. J. W. R. Teo and Y. F. Sun, Spalling behavior of interfacial intermetallic compounds in Pb-free solder joints subjected to temperature cycling loading. *Acta Materialia* 56, 242 (**2008**).

36. Y. Li and Y. C. Chan, Effect of silver (Ag) nanoparticle size on the microstructure and mechanical properties of Sn58Bi–Ag composite solders. *J. Alloys Compd.* 645, 566 (**2015**).

37. L. C. Tsao, C. H. Huang, C. H. Chung, and R. S. Chen, Influence of TiO_2 nanoparticles addition on the microstructural and mechanical properties of Sn0.7Cu nano-composite solder. *Mater. Sci. Eng., A* 545, 194 (**2012**).

38. A. F. Abd El-Rehim and M. A. Mahmoud, Transient and steady state creep of age-hardenable Al-5 wt% Mg alloy during superimposed torsional oscillations. *Journal of Materials Science* 48, 2659 (**2013**).

39. P. Wollgramm, D. Bürger, A. B. Parsa, K. Neuking, and G. Eggeler, The effect of stress, temperature and loading direction on the creep behaviour of Ni-base single crystal superalloy miniature tensile specimens. *Materials At High Temperatures* 33, 346 (**2016**).

40. S. G. Desmarest, Reliability of Pb-free solders for harsh environment electronic assemblies. *Materials Science and Technology* 28, 257 (**2012**).

41. L. Shen, Y. Wu, S. Wang, and Z. Chen, Creep behavior of Sn–Bi solder alloys at elevated temperatures studied by nanoindentation. *Journal of Materials Science: Materials in Electronics* 28, 4114 (**2017**).

42. R. Mahmudi, A. R. Geranmayeh, M. Bakherad, and M. Allami, Indentation creep study of lead-free Sn–5%Sb solder alloy. *Mater. Sci. Eng., A* 457, 173 (**2007**).

43. M. M. El-Bahay, M. E. El Mossalamy, M. Mahdy, and A. A. Bahgat, Some mechanical properties of Sn–3.5Ag eutectic alloy at different temperatures. *Journal of Materials Science: Materials in Electronics* 15, 519 (**2004**).

44. S. W. Chung, H. Watanabe, W. J. Kim, and K. Higashi, Creep deformation mechanisms in coarse-grained solid solution Mg alloys. *Materials Transactions* 45, 1266 (**2004**).

45. T. Chen, I. Dutta, and S. Jadhav, Effect of Ag and Cu concentrations on creep of Sn-based solders, *Proceedings of IPACK2007*, July 8–12 British Columbia, Canada (**2007**), pp.1–7.